Nigerian Journal of Technology (NIJOTECH)
Vol. 40, No. 6 November, 2021, pp1072 –1078
www.nijotech.com

Print ISSN: 0331-8443
Electronic ISSN: 2467-8821
http://dx.doi.org/10.4314/njt.v40i6.9

Improving Power Transfer in Rectenna Via Impedance Matching at GHz Frequencies

D. Etor[1,*], N. B. Gafai[2], I. A. Akintunde[3], O. O. Awodiji[4], L. E. Dodd[5]

[1, 3, 4] *Department of Electrical and Electronics, Faculty of Engineering, University of Jos, Plataeu State, NIGERIA*
[2]*Department of Electrical and Computer, Faculty of Engineering, Baze University, Abuja, NIGERIA*
[5]*Smart Materials and Surfaces Laboratory, Faculty of Engineering and Environment, Northumbria University, Newcastle Upon-Tyne, UNITED KINGDOM*

Abstract
A simple and elegant impedance-matching method for rectenna operating in a narrow frequency range is presented. The method used two coplanar strip lines emerging from the antenna feed-point, to correct for the reactive component of the antenna impedance on one side, and to connect the rectifier and transform its impedance on the other side. The experimental results were supported by numerical simulations, which suggest that the same impedance matching technique can be used for mm-waves and terahertz (THz) radiation applications. Microwave characterization of the fabricated devices (impedance-matched and non-matched) showed that the responsivity of the impedance-matched rectenna is approaching an order of magnitude higher at 20 GHz than that of a control device without a matching network.

Keywords: Rectenna, Impedance-matching, Coplanar strip lines, Open-circuit stub, Molecular rectifier.

1.0 INTRODUCTION

Rectennas have attracted significant attention for a variety of high-frequency applications such as sensing, power transfer, and energy harvesting [1–11]. A rectenna is a rectifier coupled to an antenna, which can convert electromagnetic radiation to an electrical DC signal. Fast rectifiers, such as the Schottky diode [2], the metal-insulator-metal (MIM) diode [1, 3–4], and more recently the self-switching nanodiode [5, 12], are often used in these applications due to their ability to operate at frequencies well into the terahertz range. One of the major drawbacks of these devices, however, is the relatively low external power conversion efficiency, caused mainly by the mismatch between the impedance of the antenna (typically 10 to 100 Ω) and that of the rectifier, often as high as several kilo-ohms [5–6, 13]. This problem can be minimized significantly by incorporating in the rectenna device a structure for matching the impedance of the rectifier to that of the antenna.

***Corresponding author **(Tel:** +234 (0) 8024362335**)**
Email addresses: etord@unijos.edu.ng (D. Etor), najashi.gafai@bazeuniversity.edu.ng (N. B. Gafai), akintundei@unijos.edu.ng (I. A. Akintunde), awodijio@unijos.edu.ng (O. O. Awodiji), linzi.dodd@northumbria.ac.uk (L. E. Dodd).

Here we report on the experimental results and numerical simulations of a simple and effective structure for matching the impedance of a self-complementary bow-tie antenna to a rectifier with a zero-bias resistance of 10 - 20 kΩ.

The device operates as a high-efficiency rectenna, which can be used in applications where efficient narrow-band operation is required, such as electromagnetic wave sensing, radio frequency identification (RFID) devices and energy harvesting (with optimized dimensions), as well as to maximise the signal-to-noise ratio in detection and imaging systems.

2.0 NUMERICAL SIMULATION RESULTS AND DISCUSSIONS

The method for transforming the equivalent antenna impedance seen by the diode relies on two coplanar strip lines connected to the antenna feed-point, as shown in Fig. 1. The characteristic impedance and propagation velocity on the lines are adjusted by changing their widths and gaps. The lines' lengths are optimized, using MATLAB Optimization toolbox, in order to transform the impedance on the antenna to the complex conjugate of the rectifier impedance, resulting in maximum power transfer [14–15].

The function of the top line is that of an open-

circuit stub of length L_{STUB}, whose susceptance B_{STUB} is in parallel to the antenna admittance Y_A. The line on the bottom, of length L_{FEED}, connects the diode to the antenna, and transforms the antenna-stub admittance to match the complex conjugate admittance of the diode Y_D so that:

$$Y_L = Y_D^* = \left[Y_0 \left(\frac{1 - \Gamma e^{-2ikL_{FEED}}}{1 + \Gamma e^{-2ikL_{FEED}}} \right) \right] \quad (1)$$

where

$$\Gamma = \frac{Y_0 - Y_A - iB_{STUB}}{Y_0 + Y_A + iB_{STUB}} \quad (2)$$

Γ is the reflection at the antenna feed-point,

$$B_{STUB} = Y_0 \tan kL_{STUB} \quad (3)$$

is the open-circuit stub susceptance, and Y_0 and k are the characteristic admittance and phase velocity of the coplanar strip lines, respectively.

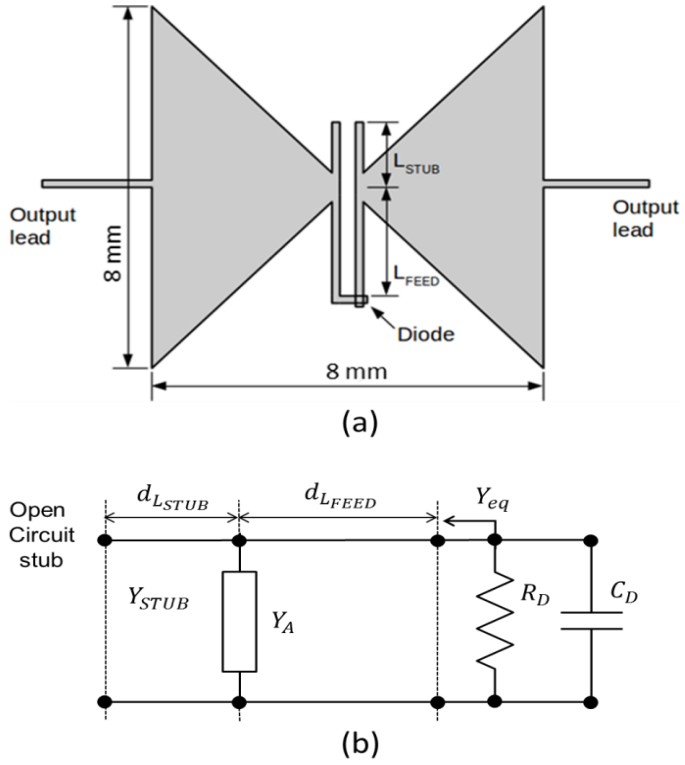

Figure 1: Layout of the model rectenna and matching structure discussed in the text operating at microwave frequencies (a). The rectenna consists of a self-complementary bow-tie and a rectifier. (b) is the equivalent circuit diagram of the device.

A model rectenna operating at microwave frequencies was designed with the self-complementary bow-tie antenna shown in Fig. 1. The substrate was a low-loss borosilicate glass substrate (dielectric constant (ε_r) = 4.6, loss tangent ($tan\ \delta$) = 3.7 x 10^{-3}, all measured at room temperature and at a frequency of 1 MHz). The antenna and lines consists of a bilayer of titanium and gold with a combined thickness of 130 nm and an overall dc conductivity of 433 x 10^3 S/m. A metal-insulator-metal (MIM) junction we recently developed was used as a rectifier in the rectenna device. The MIM junction consists of titanium and platinum electrodes with the self-assembled monolayer (SAM) octadecyltrichlorosilane (OTS) as an insulator. The detail of the diode fabrication and electrical characterization can be found in [16]. The antenna and coplanar strip lines were modelled and simulated using Agilent Advance Design System (ADS).

The geometry for the coplanar strip lines, which prevents significant amount of radiation losses from occurring in the structure, was first determined. The geometry of the lines (i.e. the gap between the two parallel lines, length and width of the lines) affects the line parameters [14–15], such as characteristic impedance and wave propagation velocity, which are required to design the matching structure. Also, the finite resistance per unit length of the electrode used for the lines results in power loss, and needs to be accounted for in order to decouple the losses due to the lines from those due to the substrate used. The measure of losses in the lines can be determined from the propagation constant [17]:

$$\gamma = \alpha + i\beta \quad (4)$$

where α is the attenuation constant and β the propagation velocity. The attenuation constant shows the measure of loss in the line [18].

As can be seen in Fig. 2(a), the attenuation in the coplanar strip lines decreases as the gap (S) between the lines increases, which was expected because, as can be seen in Fig. 2(b), the line characteristic impedance (Z) increases with increase in the gap (S). As the characteristic impedance increases, current flowing across the line decreases, hence the decrease in losses.

The coplanar strip lines width (W) and gap (S) were chosen to both be 10 μm, which were a good compromise between the line characteristic impedance and losses, as well as fringe capacitances introduced by the line ends. The line dimensions are also compatible with most photolithography equipment and relatively easy to manufacture accurately. The characteristic impedance (Z), propagation velocity (β) and attenuation (α), as simulated using the dimensions above, are plotted as a function of frequency in Fig. 3.

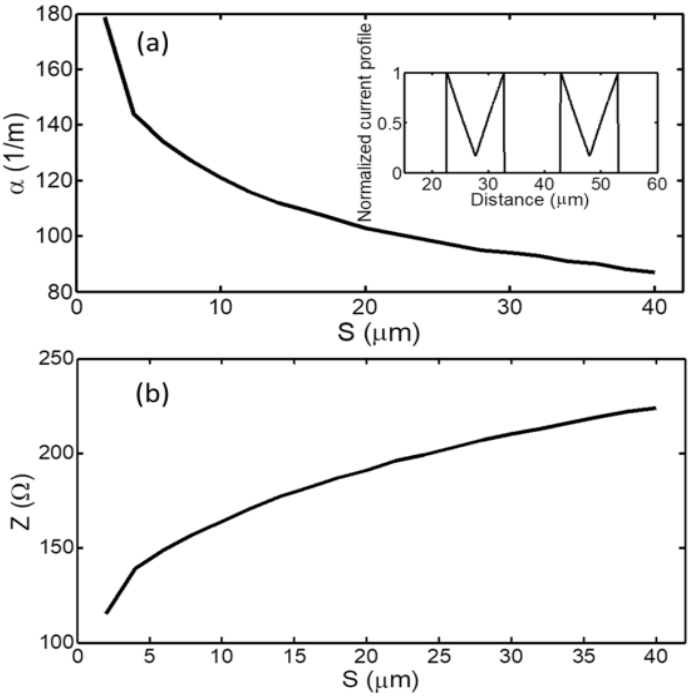

Figure 2: (a) Plot of transmission line attenuation as a function of gap between the parallel lines, and (b) line characteristic impedance as a function of gap between the parallel lines. In the inset of (a) is the typical normalized current profile of the coplanar strip lines. Operating frequency was constant at 20 GHz for both plots.

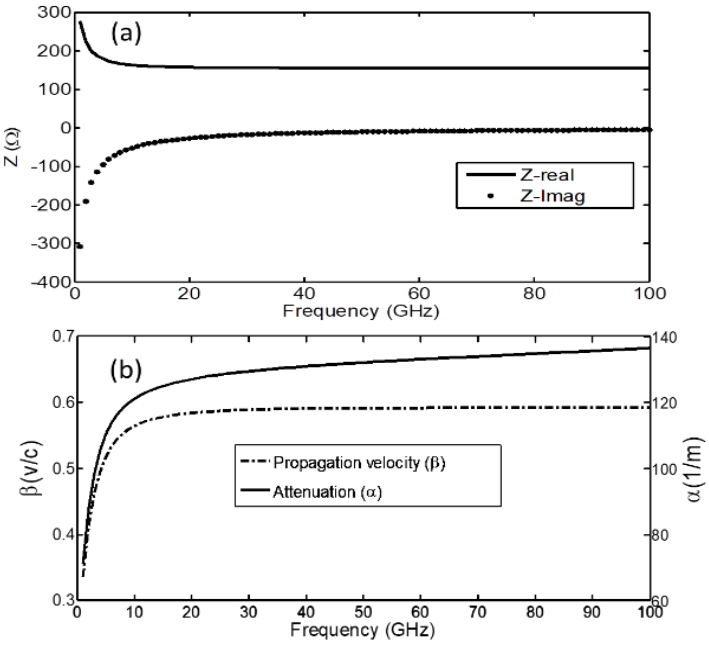

Figure 3: (a) Plot of the coplanar strip line characteristic impedance, and (b) attenuation and propagation velocity as a function of frequency. The attenuation increases in value with increasing frequency due to dielectric losses and skin effect.

As can be seen, the plotted line parameters show that the line functions well, with the propagation velocity (β) at approximately 0.6c at frequencies above 5 GHz. At lower frequencies, the real part of the line characteristic impedance (Z) can be seen (Fig. 3(a)) to be increasing as the imaginary part decreases. This was expected because, as conductance (G) decreases, the line characteristic impedance (Z) increases accordingly (Eq. 5) [15].

$$Z = \sqrt{\frac{R + j\omega L}{G + j\omega C}} \tag{5}$$

where R is the resistance, L is the inductance, G is the conductance and C the capacitance of the line.

Although the experimental work focuses only on a device operating at microwave frequencies, this technique can be ported to devices operating at terahertz frequencies, as demonstrated by Fig. 4. The coplanar strip lines design was modelled with the same electrical parameters as above, but a GaAs substrate ($\varepsilon_r \approx 10.89$), rather than glass ($\varepsilon_r \approx 4.6$) was used. GaAs is a typical substrate used for terahertz Applications.

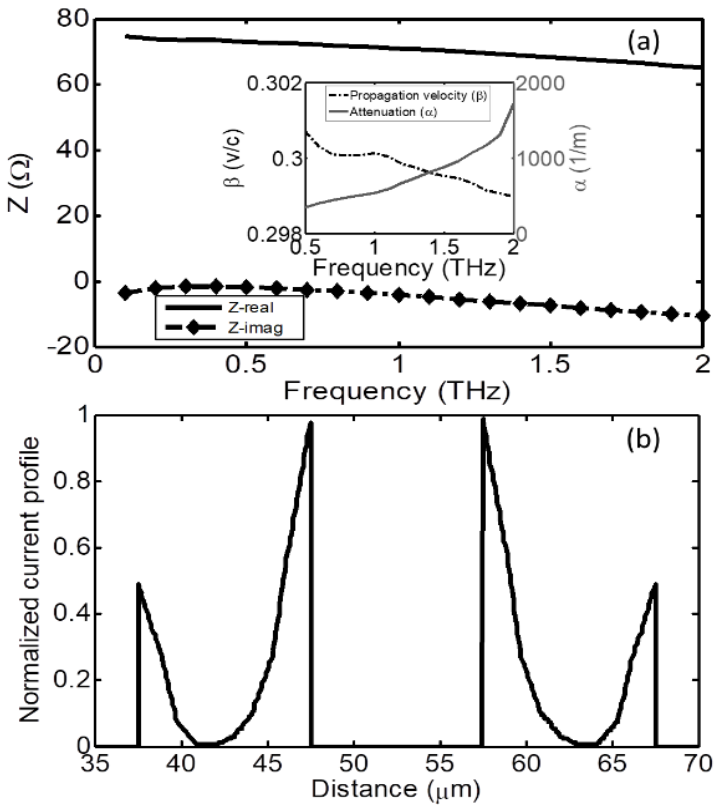

Figure 4: (a) Plot of the terahertz coplanar strip line characteristic impedance, and (b) the normalized current profile of the line. In the inset of (a) is the plot of radiation attenuation, and propagation velocity as a function of frequency.

The initial line lengths used for the microwave-

frequencies matching structure were determined by solving Eqs. (1)–(3) using MATLAB. The design was then imported into ADS for the simulation of the device impedance and radiation pattern. The optimal matching, as obtained from the MATLAB solutions, was found for L_{STUB} = 2.26 mm and L_{FEED} = 2.74 mm, dimensions which keep the overall structure compact and introduced only a negligible loss of 0.2 dB in the lines.

The computed antenna impedance at 20 GHz prior to the introduction of the impedance matching structure (i.e. the coplanar strip lines) was $Z_A = 97 + i15\ \Omega$ as can be seen in Fig. 5(a), whereas the diode impedance was to be $Z_D = (10 + i0.01)\ \text{k}\Omega$, estimated using the diode junction area and *I–V* characteristics. If no matching network were used, a 96% power loss would result due to reflections.

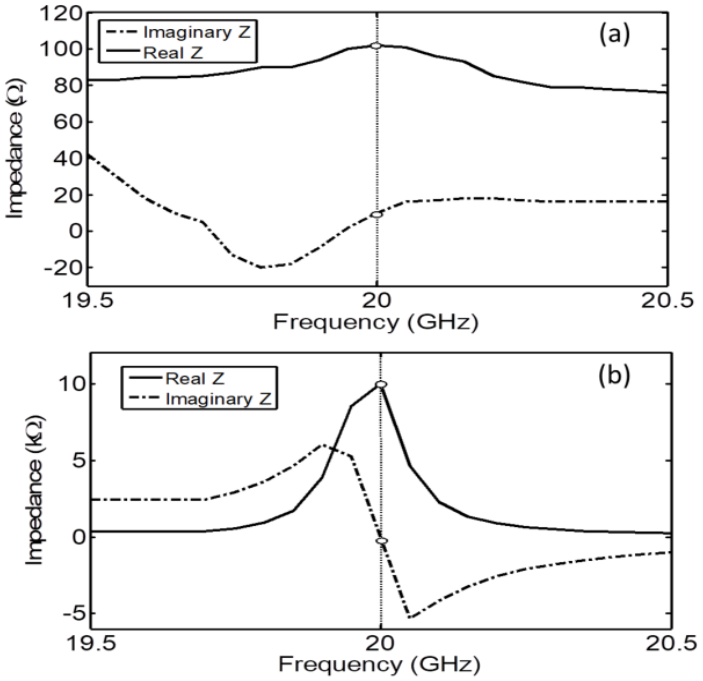

Figure 5: A plot of the designed self-complementary bow-tie antenna computed impedance as a function of frequency; (a) before, and (b) after embedding the coplanar strip lines. The impedances are Z_A = 97 + *i*15Ω and Z_A = (10 + *i*0.01) *k*Ω respectively, at 20 GHz.

The matching network developed with the technique above was a narrowband. As expected, after incorporating the matching structure (i.e. L_{STUB} and L_{FEED}) into the layout, the antenna exhibited a narrowband behavior (3dB bandwidth (BW) of 243 MHz and fractional bandwidth (FBW) of 1.2%) where the desired impedance $Z_A = (10 + i0.01)\ \text{k}\Omega$ was only obtained at a frequency of 20 GHz (see Fig. 5(b)). Potentially, a broadband impedance matching technique, which involves more complex structure with multiple transmission lines, for example the Chebyshev transformer [9], can be developed.

3.0 EXPERIMENTAL RESULTS AND DISCUSSION

3.1 Device fabrication and microwave characterisation

The control rectenna without a matching network and the rectenna with a matching network were fabricated on a 2 inch borosilicate glass substrate. The antenna patterns were transferred onto the glass substrate by conventional photolithography. A bi-layer of titanium and of gold with a combined thickness of 130 nm was then deposited as the antenna conducting metal sheet by e-beam evaporation. The gold was selectively etched at the antenna feed-point for the control unmatched structure, and at the coplanar strip line (L_{FEED}) ends for the impedance-matched structure, leaving the titanium at those areas exposed. The exposed titanium was then coated with OTS followed by the deposition of a layer of platinum with a thickness of 40 nm by e-beam evaporation, resulting in the Ti/OTS/Pt junctions. The MIM diode detail fabrication process and OTS deposition can be found in [16]. We have reported the fabrication of the Ti/OTS/Pt MIM device on a flexible plastic substrate in [19]. Fig. 6 shows the fabricated control unmatched and impedance-matched rectenna devices.

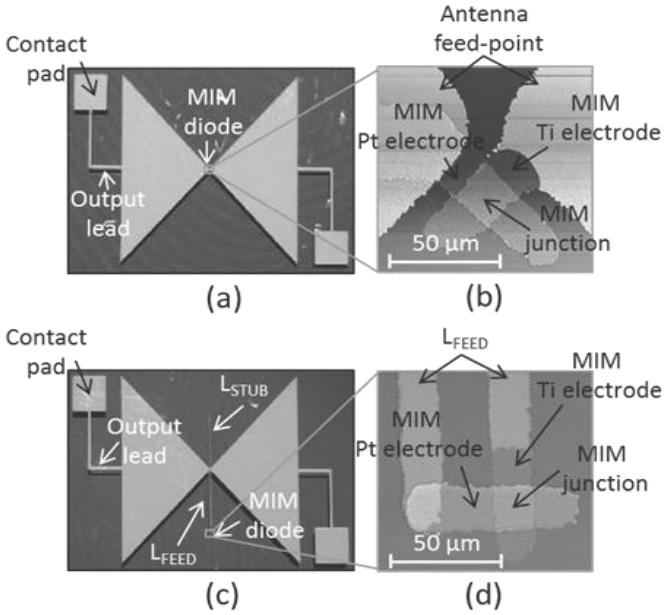

Figure 6: Optical image of the fabricated rectenna devices. (a) Is the control unmatched device, (b) is an atomic force microscopy (AFM) image showing the MIM rectifier connected to the unmatched antenna feed-point, (c) is the matched device with the matching network (coplanar strip line) visible, and (d) is an AFM image showing the MIM rectifier connected to the coplanar strip line ends of the matched device.

Microwave tests were performed on the two rectenna topologies using a vector network analyser

(VNA) as a power source. The VNA was calibrated using a power meter. A broadband antenna was connected to one of the VNA ports and a mechanical chopper with large apertures was used to intermittently illuminate the rectenna while the signal was read out using a lock-in amplifier. All measurements were performed at room temperature.

The fabricated device radiation pattern was first measured and compared with that of the simulated model. As expected, the normalized responsivity has a maximum at the normal incidence as $\theta = 0$; and the experimental data were in a relatively good agreement with the simulated data, as can be seen in Fig. 7.

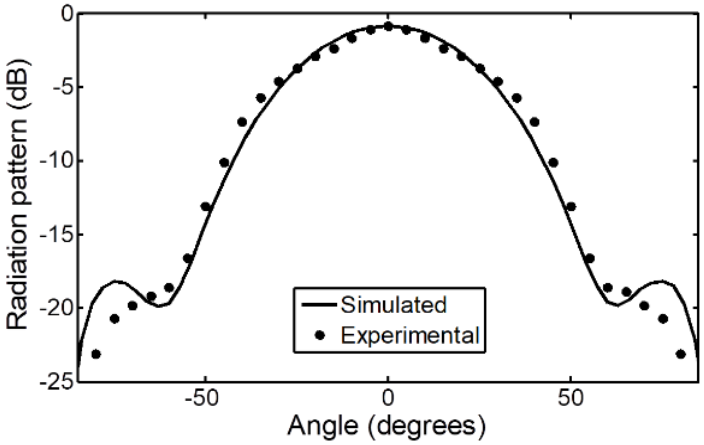

Figure 7: Measured and simulated radiation pattern of the rectenna device in H-plane.

Voltage responsivity of the two rectenna topologies was measured over a frequency range of 19 GHz to 21 GHz (the frequency region that the matching technique was implemented), and a fixed microwave source power of 32 mW (15 dBm). As can be seen in Fig. 8, the impedance-matched device produced a voltage responsivity of over 6 times higher than the unmatched device. The difference in the responsivity of the two device topologies was calculated by taking the ratio of the responsivity of the matched to that of the unmatched device, and is plotted in the inset of Fig. 8.

The rectenna devices were expected to rectify more current than they did here but it was found that the conduction mechanisms responsible for transporting electrons in the OTS dielectric layer of the Ti/OTS/Pt MIM structure is dominated by emissions other than direct tunneling, which is a faster conduction mechanism [20]. This is responsible for the reduced rectified current by the rectenna devices.

The voltage and current responsivity of the devices were further tested at source power ranging from 0.32 mW to 32 mW (-5 dBm to 15 dBm). Figs. 9(a) and 9(b) show the plot of the measured voltage and current responsivity of the two device topologies as a function of source power (with operating frequency kept constant at 20 GHz). As can be seen, the responsivities increased linearly with an increase in the source power. Also, the approximately one order of magnitude difference in the responsivities between the matched and unmatched devices can be seen at the source power of 32 mW (15 dBm).

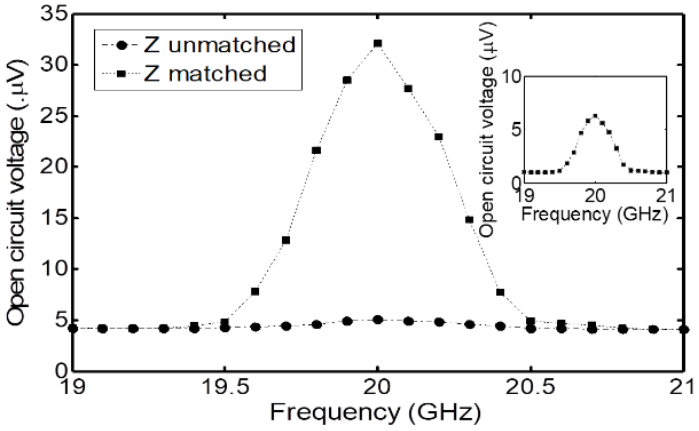

Figure 8: Plot of voltage responsivity as a function of frequency for the impedance-matched and unmatched rectennas. In the inset is the difference between the outputs of the two device topologies. The operating source power was kept constant at 32 mW (15 dBm).

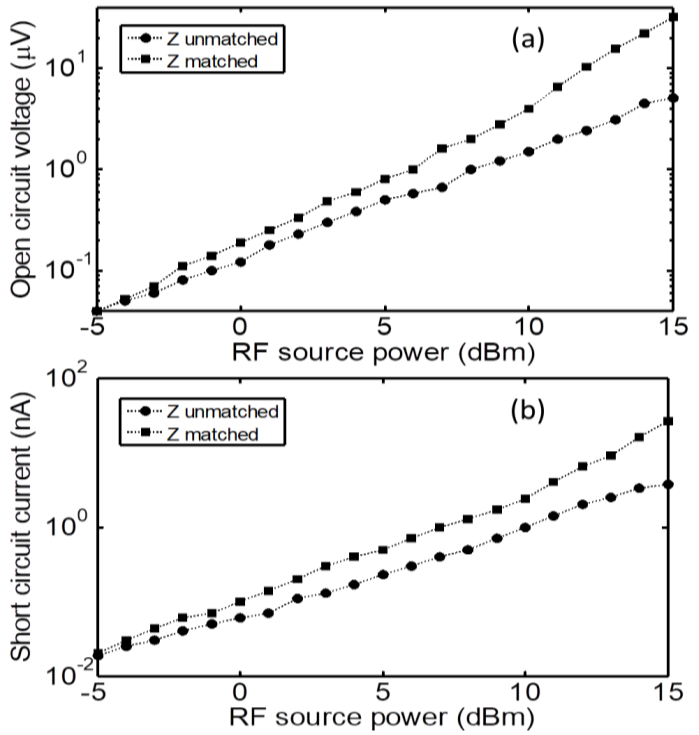

Figure 9: Plots of measured (a) voltage responsivity, and (b) current responsivity as a function of source power for the matched and unmatched devices. The operating frequency was kept constant at 20 GHz.

The effective area of the radiating antenna and of the antennas used in the two rectenna topologies is the same. The antenna gains, line losses, and actual power being radiated and absorbed by the radiating and receiving antennas respectively are irrelevant for the purpose of this work, as we are only interested in the relative difference in the rectified voltage between the unmatched and matched rectenna devices. Measurements were performed on the two rectenna topologies with the same set-up and under the same conditions.

4.0 CONCLUSION

A simple and effective technique to match the low impedance of an antenna to the high impedance of a fast rectifier has been modelled, implemented experimentally and tested in zero-bias sensing rectennas. In the model, the matching network overcame the approximately 96% power loss due to impedance mismatch between the antenna and rectifier. Experimental results showed that the impedance-matched device produced a dramatically enhanced responsivity when compared with the unmatched device, with a difference of responsivity of almost an order of magnitude between the two topologies. The design is suitable for narrow-band electromagnetic sensing applications, which, combined with optimised MIM junctions, can extend up to THz frequencies.

REFERENCES

[1] Drullinger, R. E., Evenson, K. M., Jennings, D. A., Petersen, F. R., Bergquist, J. C., Burkins, L. and Daniel, H.U. "2.5 THz Frequency Difference Measurements in the Visible Using Metal-Insulator-Metal Diodes", *Applied Physics Letters*, 42, 1983, pp.137-138, , https://doi.org/10.1063/1.93852.

[2] Hesler, J. L. and Crowe, T. W. "NEP and Responsivity of THz Zero-Bias Schottky Diode Detectors", *32nd International Conference on Infrared, Millimeter, and Terahertz (IRMMW)*, pp. 844-845, 2007, https://doi.org/10.1109/ICIMW.2007.4516758

[3] Siemsen, K. J. and Riccius, H. D. "Experiments with Point-Contact Diodes in the 30-130 THz Region" *Applied Physics Letters, A*, 35, 1984, pp. 177-187, https://doi.org/10.1007/BF00616972.

[4] Bareiß, M., Krenz, P. M., Szakmany, G. P., Tiwari, B. N., Kälblein, D., Orlov, A. O., Bernstein, G. H., Scarpa, G., Fabel, B., Zschieschang, U., Klauk, H., Porod, W., and Lugli, P. "Rectennas Revisited", *Transactions on Nanotechnology. Nanotechnology*, 12(6), 2012, pp. 1-4. https://doi.org/10.1109/TNANO.2013.2281373

[5] Pan, Y., Powell, C. V., Song, A. M. and Balocco, C. "Micro Rectennas: Brownian Ratchets for Thermal-Energy Harvesting", *Applied Physics Letters* 105, 253901, 2014, https://doi.org/10.1063/1.4905089

[6] Lee, C. H., and Chang, Y. H. "Design of a broadband circularly polarized rectenna for microwave power transmission", *Microwave and Optical Technology of Letters*, 57, 2015, pp. 702-706, https://doi.org/10.1002/mop.28931

[7] Georgiadis, A. Vera, G. A. and Collado, A. "Rectenna Design and Optimization Using Reciprocity Theory and Harmonic Balance Analysis for Electromagnetic (EM) Energy Harvesting," *Institute of Electrical and Electronics Engineers Transaction Antennas Wireless Propagation Letters, 9*, 2010, pp. 444-446, https://doi.org/10.1109/LAWP.2010.2050131.

[8] Wagih, M. Weddell, A. S. and Beeby, S. P. "Rectennas for Radio-Frequency Energy Harvesting and Wireless Power Transfer: A Review of Antenna Design [Antenna Applications Corner]," *Institute of Electrical and Electronics Engineers Transaction Antennas Propagation Magazine*, 62(5), 2020, pp. 95-107, 2020, https://www.x-mol.com/paperRedirect/1315426584495362048

[9] Shi, Y. Jing, J. Fan, Y. Yang, L. Li, Y. and Wang, M. "A novel compact broadband rectenna for ambient RF energy harvesting," *AEU International Journal of Electronics and Communication*, 95, 2018, pp.264-270, https://doi.org/10.1016/j.aeue.2018.08.035

[10] Assimonis, S. D. Fusco, V. Georgiadis, A. and Samaras, T. "Efficient and Sensitive Electrically Small Rectenna for Ultra-Low Power RF Energy Harvesting," *Sci. Rep.* 8, 15038, 2018, https://doi.org/10.1038/s41598-018-33388-w

[11] Anh, H. V. N. Thien, N. M. Trinh, L. H. Vu, T. N. and Ferrero, F. "Compact Dual-Band Rectenna Based on Dual-Mode Metal-Rimmed Antenna," *Electron.* 9(9), 1532, 2020, https://doi.org/10.3390/electronics9091532

[12] Ghaziasadi, H. Jamasb, S. Nayebi, P. and Fouladian, M. "Effect of side gates doping on graphene self-switching nano-diode rectification," *Material Research Express:* 6, 075012, 2019, https://doi.org/10.1088/2053-1591/ab10d4

[13] Choi, K., Yesilkoy, F., Ryu, G. Cho, S. H., Goldsman, N., Dagenais, M. and Peckerar, M. "A Focused Asymmetric Metal–Insulator–Metal Tunneling Diode: Fabrication, DC Characteristics

and RF Rectification Analysis," *Institute of Electrical and Electronics Engineers Transaction on Electron Devices*, 58(10), 2011, pp. 3519-3528, https://doi.org/10.1109/TED.2011.2162414

[14] Jones, E. M. T. and Bolljahn, J. T. "Coupled-Strip-Transmission-Line Filters and Directional Couplers," *Iconic Research and Engineering Transaction on Microwave Theory and Technology* 4(2), 1956, pp. 75-81, https://doi.org/10.1109/TMTT.1956.1125022

[15] Pozar, D. M. "Transmission Line Theory," in Microwave Engineering, 4th ed. Wiley, New York, pp. 48–51, 228–271, 2011

[16] Etor, D. Dodd, L. E. Wood, D. and Balocco, C. "An Ultrathin Organic Insulator for Metal–Insulator–Metal Diodes," *Institute of Electrical and Electronics Engineers Transactions on Electron Devices*, 63(7), 2016, pp. 2887–2891, https://doi.org/10.1109/TED.2016.2568279

[17] Eisenstadt, W. R. and Eo, Y. "S-Parameter-Based IC Interconnect Transmission Line Characterisation," *Institute of Electrical and Electronics Engineers Transactions Components, Hybrids, Manufacturing Technology* 15(4), 1992, pp. 428-490, https://doi.org/10.1109/33.159877

[18] Frankel, M. Y., Gupta, S., Valdmanis, J. A. and Mourou, G. A. "Terahertz Attenuation and Dispersion Characteristics of Coplanar Transmission Lines," *Institute of Electrical and Electronics Engineers Transaction Microwave Theory Technology*, 39(6), 1991, pp. 910-916, https://doi.org/10.1109/22.81658

[19] Etor, D. Dodd, L. E. Wood, D. and Balocco, C. "High-performance rectifiers fabricated on a flexible substrate," *Applied Physics Letter.*, 109, 2016, 193110, https://doi.org/10.1063/1.4967190

[20] Etor, D., Dodd, L. E., Balocco, C. and Wood, D. "Conduction mechanisms in metal/self-assembled monolayer/metal junctions," *Institution of Engineering Technology, Micro and Nano Letters*, 14(7), 2019, pp. 808 – 811, https://doi.org/10.1049/mnl.2018.5747.